Input Impedance Characteristics of Coaxial Slot Antennas for Interstitial Microwave Hyperthermia

David W.-F. Su and Lin-Kun Wu, *Member, IEEE*

***Abstract*— In this paper, a transmission-line type of input impedance model originally developed by King *et al.* [4] for the insulated dipole antenna embedded in a homogeneous dissipative medium is extended to the case of insulated coaxial slot antenna. Physical construction of the latter indicates the presence of additional current path(s) inside the feed line, which shall lead to the shortening of its resonance length. This effect is taken into account in the impedance model and verified by experiments. Furthermore, a simple strategy for optimizing the applicator's impedance-matching performance is also described and verified. Excellent agreements observed between theoretical and measured S_{11} data indicate that these models can be relied upon when designing an efficient applicator for interstitial microwave hyperthermia.**

***Index Terms*— Input impedance, insulated dipole antenna, insulated coaxial slot antenna, interstitial microwave hyperthermia.**

I. Introduction

INSULATED dipole antennas (IDA's) are widely used as applicators in the interstitial microwave hyperthermia for treating deep-seated tumors and benign prostatic hyperplasia [1]–[3]. Electrical performance of the applicator is determined by both the degree of impedance matching and specific absorption rate (SAR) distribution in the surrounding tissue. Since tens of watts of microwave power is usually employed for raising tissue temperature to the hyperthermia level of 41 °C–50 °C, good impedance matching is necessary. In fact, determination of an antenna's input impedance represents the first step in designing the applicator. Once the materials to be used for the construction of antenna and insulation (i.e., catheter) are decided, impedance modeling process results in the length and current distribution characteristics of the applicator, which are then used in a field prediction process to determine the SAR distribution in the surrounding tissue.

Theoretical modeling of the characteristics of an IDA embedded in a homogeneous conductive medium was first undertaken by King *et al.* [4]. In [4], a center-fed uniformly insulated dipole was considered. An approximate transmission-line model was employed to predict an applicator's input impedance. In this model, the dipole was first treated as a lossy coaxial transmission line consisting of a two-layer insulation and a lossy outer conductor (i.e., the surrounding lossy tissue). Formulas for the calculation of a complex propagation constant and characteristic impedance for the dominant-mode current propagating along the lossy transmission line of infinite length were then derived. Finally, by considering each of the two arms of the dipole as a finite-length open-circuit terminated transmission line, a simple formula for the prediction of the input impedance of the antenna was derived. This approach was later extended to the cases of dipole with three-layer insulation [5], multisectioned dipoles [6], [7], and an asymmetrically fed dipole [8].

As was pointed out by Hurter *et al.* [9], heating performance of the conventional IDA's (see, e.g., the actual antenna structures constructed and tested in [4], [5], [7], and [8]) was insertion-depth dependent. This was due to the presence of a current that flowed backward in the direction toward the generator along the outer conductor of the feeding line. With an insufficient insertion depth, as was reported by Zhang *et al.* [8] and Hurter *et al.* [9], reflection from the air–tissue interface also affects the impedance-matching performance of the dipole. In [9], Hurter *et al.* described the use of a quarter-wavelength sleeve (which is also commonly referred to as "choke"), which, with a short-circuit termination, presented an open-circuit input impedance to terminate the above-mentioned back-flow current.

While conventional insulated dipoles were usually made from coaxial cable, a triaxial cable was employed in [9] to facilitate a simple way of constructing both the choke and the radiating part of the antenna; the structural geometry of which is depicted here as a special case to the generalized insulated antenna structure shown in Fig. 1. It is noted that a triaxial cable consists of three coaxial conductors, its center and inner conductors form an inner coaxial cable, while inner and outer conductors form an outer coaxial cable; the two coaxial cables usually have different characteristic impedances.

In this research, the method of analysis developed by King *et al.* in [4] is extended further to model the input impedance characteristics of a coaxial slot antenna (CSA) type of insulated applicator. Specifically, two CSA's, both constructed from triaxial cable, are considered. For convenience, the three antennas will be denoted hereafter as IDA, CSA-I, and CSA-II, respectively. A generalized representation of the structural

Manuscript received March 30, 1998; revised November 16, 1998. This work was supported by the National Research Council of the Republic of China under Grant NSC 86-2213-E-009-061 and under Grant NSC 87-2213-E-009-127.

D. W.-F. Su was with the Institute of Communication Engineering, National Chiao Tung University, Hsinchu, Taiwan 30050, R.O.C. He is now with Alpha Telecom Inc., Hsinchu, Taiwan 30050, R.O.C.

L.-K. Wu is with the Institute of Communication Engineering, National Chiao Tung University, Hsinchu, Taiwan 30050, R.O.C.

Publisher Item Identifier S 0018-9480(99)01954-7.

0018–9480/99$10.00 © 1999 IEEE

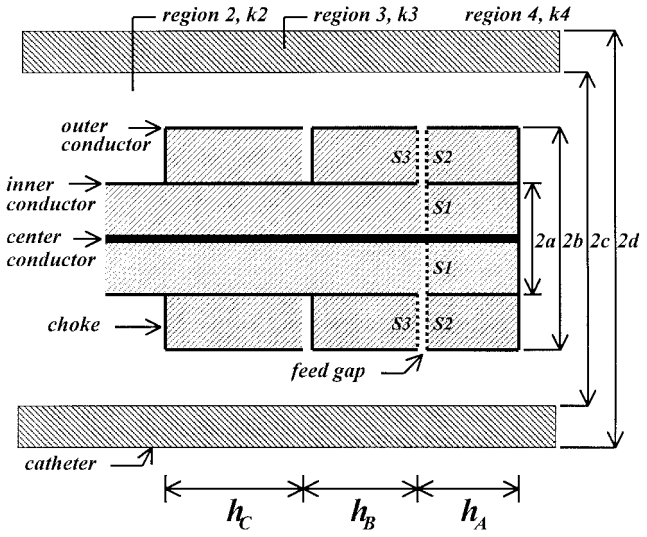

Fig. 1. Generalized geometry of IDA, CSA-I, and CSA-II antennas.

details associated with all three antennas is depicted in Fig. 1, the differences among them occur on the two sides of the feed gap. For the IDA investigated in [9], the *inner* and *outer* coaxial cables associated with section A are both short circuited (i.e., connecting them along $S1$ and $S2$) while the outer coaxial cable of section B is also shorted (i.e., $S3$ is connected). In contrast, short-circuit connections are made only over $S2$ and $S3$, but not $S1$ for CSA-I antenna. In doing so, CSA-I sees an additional impedance loading presented by the short-circuited inner coaxial cable of length h_A, which is not present in the IDA. Aside from this, both antenna structures share the same section B (which is formed by connecting the inner and outer conductors of the triaxial cable at both ends) and choke (which is simply a quarter-wavelength section of the short-circuited outer coaxial cable).

As will be shown in Section III, the short-circuited inner coaxial feed line found in CSA-I represents an extra current path, which results in a reduction of the resonant length of the antenna; this, as will be described in a separate paper, further affects the heating performance of the CSA's. This length-reduction feature is exploited further by the CSA-II antenna. As oppose to IDA and CSA-I, $S1$, $S2$, and $S3$ are left unconnected for the CSA-II antenna to obtain additional internal current paths.

In Section II, approximate transmission-line types of the impedance model are derived for the three antennas shown in Fig. 1. These models are then used to determine each antenna's structural parameters for theoretically yielding a better than -10 dB of $|S_{11}|$ at the industrial, scientific, and medical (ISM) frequency of 915 MHz. Corresponding antennas are then constructed and tested, with theoretical and experimental results presented and compared in Section III. Concluding remarks are presented in Section IV.

II. Method of Analysis

A. IDA

According to the theory of insulated antenna in a conducting or lossy dielectric medium developed by King *et al.* [4],

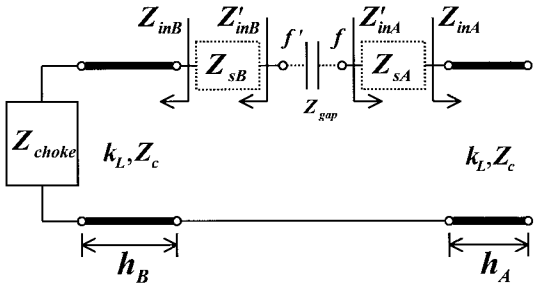

Fig. 2. Generalized equivalent circuit used for the modeling of the input impedance of IDA, CSA-I and CSA-II antennas shown in Fig. 1. For IDA, Z_{sA} and Z_{sB} are absent. For CSA-I, Z_{sB} is removed. For CSA-II, Z_{sA} and Z_{sB} are retained.

design and analysis of these antennas in conductive media may be proceeded by first treating the two radiating portions of the antenna as finite-length lossy transmission lines, the input impedances of which are denoted as $Z_{\text{in}A}$ and $Z_{\text{in}B}$, respectively. These, for the generalized equivalent circuits shown in Fig. 2, which are applicable to all three antennas investigated here, are obtained by simply setting Z_{sA} and Z_{sB} to zero. According to King [10], the gap capacitance Z_{gap} may be ignored such that the input impedance of the antenna appearing across the terminals $f - f'$ can be approximated as

$$Z_{\text{in}} = Z_{ff'} \cong Z_{sA} + Z_{sB} \tag{1}$$

where $Z_{\text{in}A}$ and $Z_{\text{in}B}$ are given by

$$Z_{\text{in}A} = -jZ_c/\tan(k_L h_A) \tag{2a}$$

$$Z_{\text{in}B} = Z_c \frac{Z_{\text{choke}} + jZ_c \tan(k_L h_B)}{Z_c + jZ_{\text{choke}} \tan(k_L h_B)}. \tag{2b}$$

The complex wavenumber $k_L (= \beta_L - j\alpha_L)$ and the characteristic impedance of the lossy transmission line Z_c appearing in (2) are given by [4]

$$k_L = k_2 \left[\frac{\ln(d/b)}{\ln(c/b) + n_{23}^2 \ln(d/c)}\right]^{1/2} \left[\frac{\ln(d/b) + F}{\ln(d/b) + n_{24}^2 F}\right]^{1/2} \tag{3}$$

$$Z_c = (\omega\mu_0 k_L / 2\pi k_2^2)[\ln(c/b) + n_{23}^2 \ln(d/c) + n_{24}^2 F] \tag{4}$$

where $n_{23}^2 = k_2^2/k_3^2$, $n_{24}^2 = k_2^2/k_4^2$, and $F = H_0^{(1)}(k_4 d)/k_4 \; dH_1^{(1)}(k_4 d)$. The total impedance of the choke (Z_{choke}) is defined as

$$Z_{\text{choke}} = Z_c + jZ_{02} \tan(\beta_2 h_c) \tag{5}$$

where Z_{02} and β_2 represent the TEM mode characteristic impedance and propagation constant of the *outer* coaxial cable, respectively. It is observed that Z_{choke} is assumed to be equal to the series combination of the input impedances of the short-circuited transmission line interior to the choke and the lossy transmission line exterior to the choke which, for simplicity, is assumed to be infinitely long such that its input impedance is the same as its characteristic impedance Z_c.

As a choke, h_c is chosen to be a quarter-wavelength long at the desired operating frequency of 915 MHz, which results in an infinite value for Z_{choke}. As a consequence, $Z_{\text{in}B}$ reduces to the same form as $Z_{\text{in}A}$ in (2a) (with h_A replaced by h_B).

When designing a symmetrical IDA, $h_A(=h_B)$ is chosen to be near a quarter-wavelength long to yield near pure real $Z_{\text{in}A}$ $(Z_{\text{in}B})$ and Z_{in} at 915 MHz. Alternatively, one may employ an asymmetrical IDA with proper combination of h_A and h_B to achieve better impedance matching and/or SAR characteristics.

B. Insulated CSA-I

For a CSA-I antenna, the feed current will travel first into the short-circuited transmission line in the feed cable before reaching the exterior radiating portion of section A of the antenna. The effect of this extra current path can be accounted for in the generalized equivalent circuit of Fig. 2 by keeping Z_{sA} while setting Z_{sB} to zero. As a consequence, $Z_{\text{in}A}$ given in (2a) should be modified to include an additional series term (i.e., Z_{sA}) corresponding to the input impedance of the internal short-circuited feed line. Given this, the input impedance of CSA-I antenna can be written as

$$Z_{\text{in}} = Z'_{\text{in}A} + Z_{\text{in}B} \tag{6}$$

where the modified impedance $Z'_{\text{in}A}$ is defined as

$$Z'_{\text{in}A} = Z_{sA} + Z_{\text{in}A}. \tag{7}$$

In (7), Z_{sA} represents the above-mentioned loading effect and can be easily determined by the transmission-line theory as

$$Z_{sA} = jZ_{01}\tan(\beta_1 h_A) \tag{8}$$

where Z_{01} and β_1 represent the TEM mode characteristic impedance and propagation constant of the *inner* coaxial cable, respectively.

It is important to observe that $\beta_L(=\text{Re}\{k_L\})$ is strongly influenced by k_4, while β_1 is determined by the cable insulation. With the antenna surrounded by a thin catheter and highly lossy human tissue, β_L is much larger then β_1, which points out that $\lambda_L(=2\pi/\beta_L)$ is much smaller than $\lambda_1(=2\pi/\beta_1)$. It then follows that for a CSA-I antenna, one may choose h_A (and/or h_B) to be shorter than $\lambda_L/4$ such that $Z_{\text{in}A}$ (and/or $Z_{\text{in}B}$) possesses a capacitive reactance which is compensated by the pure inductive Z_{sA} (since $h_A \ll \lambda_1/4$) to yield a purely real Z_{in} at operating frequency.

The above observation indicates that the presence of the extra current path in the inner coaxial feed line may lead to a reduction in the resonant length (i.e., $h_A + h_B$) of the antenna. This attribute can be very attractive when designing interstitial applicator for operation at lower ISM frequencies (e.g., 433 MHz), as its use may make it possible for the length of the applicator to match the longitudinal extent of solid tumors or prostate to be heated. This feature is exploited further in Section II-C.

C. Insulated CSA-II

Following the above observation, one may introduce additional current path inside the feed line to further reduce the radiating length of the antenna. For the triaxial cable used here, CSA-I antenna employs only the extra current path available in the inner coaxial cable. It is then obvious that by simply leaving the inner and outer conductors of the triaxial cable unconnected at the near end of either section A or B, or both, one or two more extra internal current path(s) become available, which should lead to the possibility of further reduction in the radiating length of the antenna. As the extreme case, both current paths are employed here for the CSA-II structure.

Following the above analysis, the equivalent circuit for CSA-II is obtained by retaining both Z_{sA} and Z_{sB}, shown in Fig. 2, from which its input impedance can be written as

$$Z_{\text{in}} = Z'_{\text{in}A} + Z'_{\text{in}B} \tag{9}$$

where $Z'_{\text{in}A}$ and $Z'_{\text{in}B}$ are given by

$$Z'_{\text{in}A} = Z_{sA} + Z_{\text{in}A} \tag{10}$$

$$Z'_{\text{in}B} = Z_{sB} + Z_{\text{in}B} \tag{11}$$

with

$$Z_{sA} = jZ_{01}\tan(\beta_1 h_A) + jZ_{02}\tan(\beta_2 h_A) \tag{12}$$

$$Z_{sB} = jZ_{02}\tan(\beta_2 h_B). \tag{13}$$

It is obvious that with

$$h_A \quad h_B < \lambda_L/4 \quad \lambda_1/4 \quad \text{and} \quad \lambda_2/4 \tag{14}$$

Z_{sA} and Z_{sB} are both purely inductive, while $Z_{\text{in}A}$ and $Z_{\text{in}B}$ both possess capacitive reactance. With proper combination of h_A and h_B, the CSA-II antenna can resonate (i.e., with pure real Z_{in}) at a much shorter length than both CSA-I and IDA antennas.

III. Results

In order to verify the accuracy of impedance models, theoretically calculated S_{11} data are compared with experimental data measured with an HP8720 vector network analyzer. Antennas are constructed with the UT 78-50-25 triaxial cable from UTI (Micro-Coax Components, Collegeville, PA.), the outer diameter of its outer conductor (i.e., $2b$ in Fig. 1) is 1.99 mm. All antennas are insulated by the same PTFE (Teflon) catheters with 2.0-mm inner diameter (i.e., $2c$) and 3.2-mm outer diameter (i.e., $2d$). They are then inserted through a predrilled hole into a solid muscle-equivalent phantom, which consists of 58.33% ethanediol, 36.67% H_2O, 1.67% NaCl, and 3.33% agar (weight percents). The dielectric properties of solid phantom, as revealed by the solid curves of Fig. 3, are measured by the HP85010 dielectric constant measurement system and are consistent with the experimental data ($\varepsilon' = 46-53$ and $\varepsilon'' = 19-25$, around 915 MHz) reported in [11]. These data are smoothed, as shown by the dotted curves in Fig. 3, before being used in the impedance models. In the following, the above structural and material parameters are fixed; h_A and h_B are then selected to yield a better than -10-dB return loss at 915 MHz for each individual antenna design.

The first set of design example is intended for the demonstration of the loading effect of the internal short-circuited line on the antenna's resonant frequency and/or resonant length. In this case, IDA and CSA-I antennas are considered. Theoretical

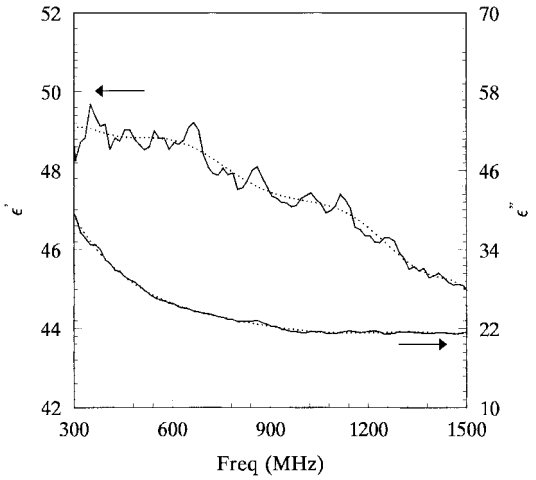

Fig. 3. Real and imaginary parts of the complex dielectric constant for the solid phantom used in the experiments. Solid line: measured data. Dotted line: smoothed data.

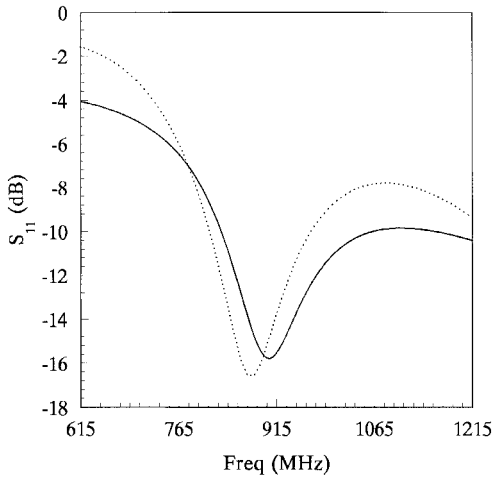

Fig. 4. Comparison of the calculated and measured return loss for the IDA with $h_A = 20$ mm and $h_B = 45$ mm. Solid line: measured data. Dotted line: calculated data.

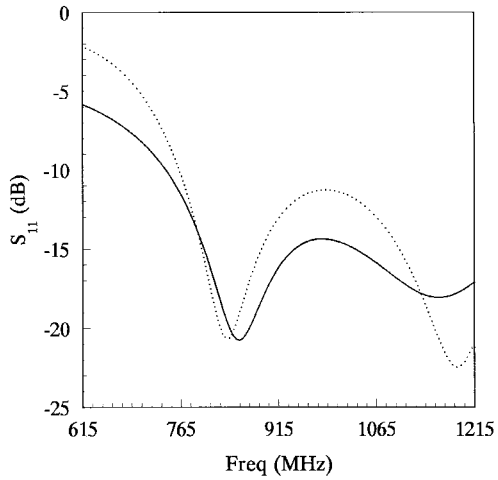

Fig. 5. Comparison of the calculated and measured return loss for the CSA-I with $h_A = 20$ mm and $h_B = 45$ mm. Solid line: measured data. Dotted line: calculated data.

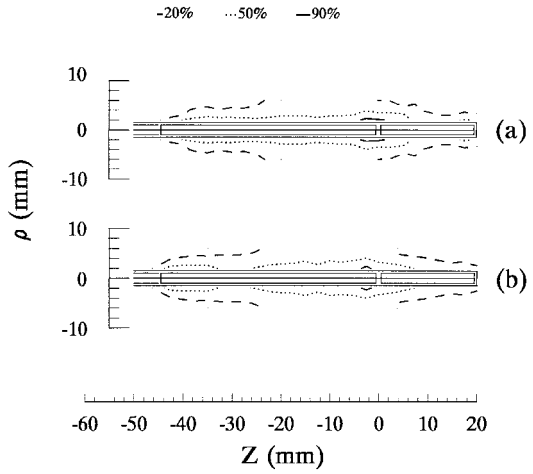

Fig. 6. Comparison of measured SAR pattern for (a) IDA and (b) CSA-I investigated in Figs. 4 and 5, respectively.

calculations indicate that, with $h_A = 20$ mm and $h_B = 45$ mm, both antennas exhibit better than -10-dB return loss at 915 MHz. The calculated and measured frequency responses of the return loss for IDA and CSA-I are shown in Figs. 4 and 5, respectively. The calculated and measured resonant frequencies are 880 and 905 MHz, respectively, for IDA, and 840 and 855 MHz, respectively, for CSA-I. In all cases, $|S_{11}| < -10$ dB are observed at the desired operating frequency of 915 MHz. The lower resonant frequency observed for CSA-I clearly indicates that, to raise its resonant frequency to near that of the IDA (or to 915 MHz), shorter h_A and/or h_B should be used. This resonant length reduction capability is obviously afforded by the presence of the extra current path inside the coaxial feed line.

The SAR patterns associated with those two antennas are also measured at 915 MHz and displayed in Fig. 6. Since fields radiated by these antennas are governed by the normalized current distributions present on the outer conductor, which are identical for the IDA and CSA-I with the same h_A and h_B, the resultant SAR patterns are quite similar. It is also noted that since the longitudinal extent of the measured SAR pattern is confined within the length of both antennas, the current choking behavior of the $\lambda/4$ sleeve is confirmed.

In the previous example, the only constraint imposed on the design of IDA and CSA-I is that better than -10 dB of return loss is obtained at 915 MHz. As shown in Figs. 4 and 5, although this requirement is satisfied in both cases, the designed antennas resonate at frequencies other than 915 MHz. Since the lowest return loss usually occurs at or near the first resonance, antenna design can be optimized by computing S_{11} at the desired operating frequency for a set of (h_A, h_B) combinations and, from which, choose the one that results in purely real S_{11} which is also small enough to meet the preset impedance matching performance (say, -10 dB).

To illustrate this process with a simplified example, we first fix h_B to 40 mm, and frequency to 915 MHz, S_{11} are then calculated for all three types of antenna as functions of h_A. With h_A varies from 1 to 100 mm, the resultant $S_{11}(h_A)$ are plotted in Fig. 7. As can be seen, for the range of h_A chosen, both CSA-II and IDA have gone through three resonances,

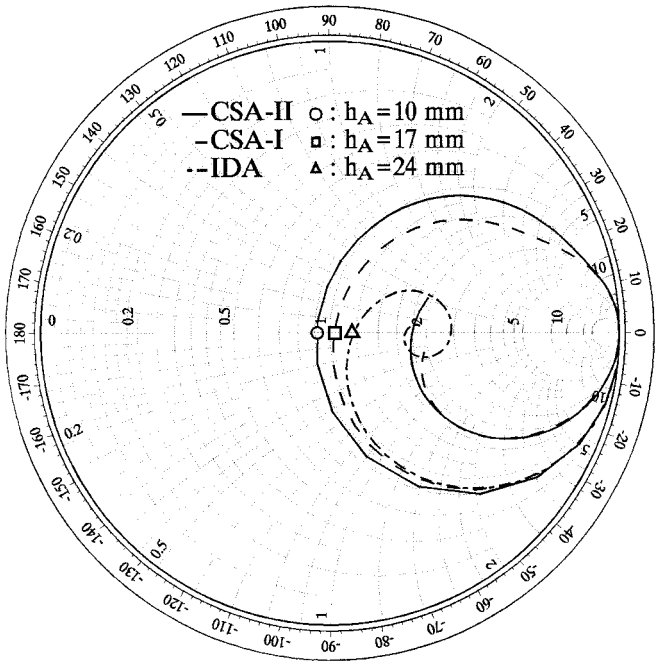

Fig. 7. Smith chart of antenna's input impedance versus h_A for $h_B = 40$ mm at 915 MHz. Solid line: CSA-II. Dash line: CSA-I. Dotted line: IDA.

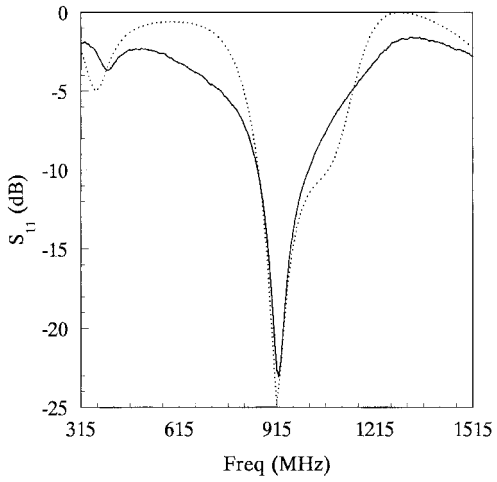

Fig. 8. Comparison of the calculated and measured return-loss data for CSA-II operating at 915 MHz with $h_A = 10$ mm and $h_B = 40$ mm. Solid line: measured data. Dotted line: calculated data.

while two resonances occurred to the CSA-I curve. These curves also indicate that the lowest $|S_{11}|$ usually occurs at or near the first resonance (especially for CSA-I and II). From this example, $(h_A, |S_{11}|)$ correspond to the first resonances are (10 mm, −24 dB), (17 mm, −33 dB) and (24 mm, −22 dB) for CSA-II, CSA-I, and IDA, respectively, which indicate that the first resonance lengths of IDA and CSA-I are longer than that of CSA-II by 28% and 14%, respectively. Since excellent $|S_{11}|$ are observed, it is not necessary to repeat $S_{11}(h_A)$ calculations for different h_B values.

This simple optimization process is exercised for the two CSA-II antennas that are designed for operation at 915 and 433 MHz, respectively. The resultant (h_A, h_B) are (10, 40 mm) and (16, 80 mm) for operation at 915 and 433 MHz, respectively. The corresponding calculated and measured $S_{11}(f)$ are shown in Figs. 8 and 9, in which good agreements between theoretical and measured data are observed, except for a slight shift in frequency response, which may be attributed to tolerances in material and structural parameters.

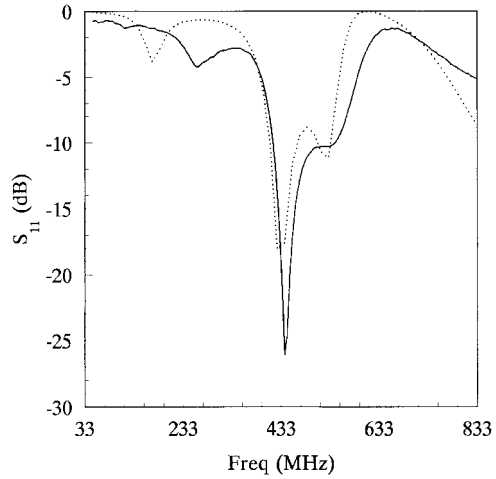

Fig. 9. Comparison of the calculated and measured return loss data for CSA-II operating at 433 MHz with $h_A = 16$ mm and $h_B = 80$ mm. Solid line: measured data. Dotted line: calculated data.

IV. Conclusions

New formulas for the predictions of the input impedance characteristics of insulated CSA's are derived in this paper. For comparison, the impedance model developed earlier by King *et al.* [4] for IDA's is also presented here. A simple strategy for the optimization of an applicator's impedance-matching performance at the desired frequency of operation is also described. Accuracy of the impedance models are confirmed by the good agreements observed between theoretically calculated and experimentally measured $S_{11}(f)$ data; the slight shift in frequency response observed between calculated and measured data may be attributed to tolerances in material and structural parameters. Therefore, these impedance models can be relied upon when designing efficient interstitial hyperthermia applicators.

With the additional current path(s) present in the internal feed line, the two CSA's, especially the CSA-II design, are found to possess shorter resonant lengths than IDA's having comparable impedance-matching performance. This length-shortening feature may be advantageously applied when designing interstitial hyperthermia applicators for operation at lower ISM frequencies, for which the radiating length required of the traditional insulated dipole applicator may be too long to match the longitudinal extent of the tissue region to be heated. Heating performance of CSA's operating at both 915 and 433 MHz will be described in a different paper.

References

[1] B. E. Lyons, R. H. Britt, and J. W. Strohbehn, "Localized hyperthermia in the treatment of malignant brain tumors using an interstitial microwave antenna array," *IEEE Trans. Biomed. Eng.*, vol. BME-31, pp. 53–62, Jan. 1984.

[2] A. M. Tumeh and M. F. Iskander, "Performance comparison of available interstitial antennas for microwave hyperthermia," *IEEE Trans. Microwave Theory Tech.*, vol. 37, pp. 1126–1133, July 1989.
[3] D. Despretz, J.-C. Camart, C. Michel, J.-J. Fabre, B. Prevost, J.-P. Sozanski, and M. Chive, "Microwave prostatic hyperthermia: Interest of urethral and rectal applicators combination-theoretical study and animal experimental results," *IEEE Trans. Microwave Theory Tech.*, vol. 44, pp. 1762–1767, Oct. 1996.
[4] R. W. P. King, B. S. Trembly, and J. W. Strohbehn, "The electromagnetic field of an insulated antenna in a conducting or dielectric medium," *IEEE Trans. Microwave Theory Tech.*, vol. MTT-31, pp. 574–583, July 1983.
[5] J.-C. Camart, J.-J. Fabre, B. Prevost, J. Pribetich, and M. Chive, "Coaxial antenna array for 915-MHz interstitial hyperthermia: Design and modelization-power deposition and heating pattern-phased array," *IEEE Trans. Microwave Theory Tech.*, vol. 40, pp. 2243–2250, Dec. 1992.
[6] P. S. Debicki and M. A. Astrahan, "Calculating input impedance of electrically small insulated antennas for microwave hyperthermia," *IEEE Trans. Microwave Theory Tech.*, vol. 41, pp. 357–360, Feb. 1993.
[7] M. F. Iskander and A. M. Tumeh, "Design optimization of interstitial antennas," *IEEE Trans. Microwave Theory Tech.*, vol. 36, pp. 238–246, Feb. 1989.
[8] Y. Zhang, N. V. Dubal, R. Takemoto-Hambleton, and W. T. Joines, "The determination of the electromagnetic field and SAR pattern of an interstitial applicator in a dissipative dielectric medium," *IEEE Trans. Microwave Theory Tech.*, vol. 36, pp. 1438–1443, Oct. 1988.
[9] W. Hurter, F. Reinbold, and W. J. Lorenz, "A dipole antenna for interstitial microwave hyperthermia," *IEEE Trans. Microwave Theory Tech.*, vol. 39, pp. 1048–1054, June 1991.
[10] R. W. P. King, "Asymmetrically driven antennas and the sleeve dipole," *Proc. IRE*, pp. 1154–1164, Oct. 1950.
[11] R. Peloso, D. T. Tuma, and R. K. Jain, "Dielectric properties of solid tumors 1during normothermia and hyperthermia," *IEEE Trans. Biomed. Eng.*, vol. BME-31, pp. 725–728, Nov. 1984.

David W.-F. Su was born in Kauhsiung, Taiwan, R.O.C., on May 9, 1968. He received the B.S. and M.S. degrees in communication engineering, and the Ph.D. degree from the National Chiao Tung University, Hsinchu, Taiwan, R.O.C., in 1990 and 1992, and 1999, respectively.

From 1992 to 1993, he was an R&D Engineer at the Taiwan Microwave Co., Ltd., where he participated in various RF and microwave-circuit-design projects. From 1993 to 1998, he was been with the Department of Communication Engineering at National Chiao Tung University, where he was engaged in microwave hyperthermia and radiometry, and traveling-wave tube and insulated antenna design. He is currently with Alpha Telecom Inc., Hsinchu, Taiwan, R.O.C., where his work mainly concerns the developments of wireless local loop and mobile communication system.

Lin-Kun Wu (S'81–M'81) was born in Hsinchu, Taiwan, R.O.C., in 1958. He received the M.S. and Ph.D. degrees in electrical and computer engineering from the University of Kansas, Lawrence, in 1982 and 1985, respectively.

From November 1985 to December 1987, he was a Post-Doctoral Research Associate at the Center for Research, Inc., University of Kansas, where he worked on microwave remote sensing and computational electromagnetics. In 1988, he joined the Department of Communication Engineering, National Chiao Tung University, Hsinchu, Taiwan, R.O.C., where he is currently a Professor. His current research interests include computational electromagnetics, biological effects and medical applications of electromagnetic energy, and electromagnetic compatibility.